IBRACON Structures and Materials Journal
Revista IBRACON de Estruturas e Materiais
ISSN 1983-4195 ismj.org

REVIEW ARTICLE

Flexural design of concrete beams reinforced with FRP rebars

Dimensionamento à flexão de vigas em concreto armado com barras de FRP

Felipe Augusto da Silva Barbosa[a]
Túlio Nogueira Bittencourt[a]
Gustavo Rodovalho Boriolo[a]
Fellipe Rodrigues André[b]
Marcos Massao Futai[a]

[a]Universidade de São Paulo – USP, Department of Structural and Geotechnical Engineering, São Paulo, SP, Brasil
[b]Universidade São Judas Tadeu – USJT, Department of Civil Engineering, São Paulo, SP, Brasil

Received 15 February 2022
Accepted 06 September 2022

Abstract: The corrosion of steel rebars is the main cause of reinforced concrete degradation, which results in increasing costs with structural rehabilitation and repairs. As a solution, corrosion resistant rebars, such as those of FRP – Fiber-reinforced polymer –, have been used to replace conventional steel. This paper describes the development of a design program that calculates the flexural FRP reinforcement of T-shape beams. The possibilities as regards the neutral axis position, failure mode and concrete linear or non-linear behavior define the design scenarios for which their respective equations were deduced. The flexural strengths computed using the deduced equations showed agreement with experimental results for 125 beams, validating the proposed methodology. Since FRP rebars are vulnerable to creep rupture, the sustained stresses must be lower than the maximum allowed by ACI 440.1R-15, which may require increases in areas, modifying the flexural strength. Therefore, the equations to compute the new neutral axis depth and flexural strength based on the adjusted area were deduced and implemented in the computational program. Subsequently, this paper presents design examples considering all scenarios for which the equations were deduced. The design of one T-section considering different FRP rebars combined to normal and high-performance concretes is also reported. The results showed that beams reinforced with aramid and glass FRP required large areas to avoid creep rupture, whereas the areas of those reinforced by carbon FRP rebars were considerably small; however, they exhibited small curvatures and fragile failure when under-reinforced.

Keywords: reinforced concrete, FRP rebars, T-sections, non-metallic reinforcement, design program.

Resumo: A corrosão do aço é a principal causa de degradação do concreto estrutural, implicando elevados custos com reabilitação e reparos. Diante disto, barras de FRP – Polímeros Reforçados por Fibras – constituem uma alternativa ao aço convencional em virtude de sua excelente resistência à corrosão. Este trabalho descreve o desenvolvimento de um programa para dimensionamento da armadura de FRP à flexão em vigas de seção T. As diferentes possibilidades referentes à posição da linha neutra, modo de falha e comportamento linear ou não-linear do concreto definem os cenários de dimensionamento para os quais se aplicam as formulações desenvolvidas. Os momentos resistentes calculados apresentaram concordância com valores obtidos experimentalmente, validando a metodologia proposta. Uma vez que as barras de FRP são suscetíveis à ruptura por fluência, tensões devido a cargas permanentes devem se manter inferiores ao limite estabelecido pelo ACI 440.1R-15, ajustando-se as áreas de armadura quando necessário. Desta maneira, foram implementadas no programa, as equações para cálculo da linha neutra e momento resistente baseadas nas áreas ajustadas. Subsequentemente, são apresentados exemplos de dimensionamento considerando os diversos cenários para os quais desenvolveram-se as formulações, combinando-se diferentes tipos de FRP a variadas classes de concreto. Os resultados mostraram que vigas T armadas com FRP de aramida e vidro exigiram elevadas áreas de armadura para atender ao estado limite de ruptura por fluência. Em contrapartida, seções armadas com FRP de carbono exigiram áreas menores, porém exibindo ruptura frágil e curvaturas reduzidas quando sub-armadas.

Palavras-chave: concreto armado, barras de FRP, seções T, armadura não-metálica, programa de dimensionamento.

How to cite: F. A. S. Barbosa, T. N. Bittencourt, G. R. Boriolo, F. R. André, and M. M. Futai, "Flexural design of concrete beams reinforced with FRP rebars," *Rev. IBRACON Estrut. Mater*., vol. 16, no. 4, e16403, 2023, https://doi.org/10.1590/S1983-41952023000400003

Corresponding author: Felipe Augusto da Silva Barbosa. E-mail: felipe.asb92@usp.br
Financial support: This study was fully financed by the Coordination for the Improvement of Higher Education Personnel (*Coordenação de Aperfeiçoamento de Pessoal de Nível Superior*) - Brazil (CAPES) - Finance Code 001 and Catedra Under Rail – VALE.
Conflict of interest: Nothing to declare.
Data Availability: Due to the nature of this research, participants of this study did not agree for their data to be shared publicly, so supporting data are not available.

1 INTRODUCTION

During the past century, the focus on obtaining high strength concretes entailed certain unconcern regarding durability issues. Somehow, the use of materials with excellent mechanical properties contributed to negligence as regards quality control at construction sites [1]. However, the degradation of structures subjected to aggressive environments as well as the increasing costs in repairs raised the discussion on how to avoid steel corrosion and preserve structural integrity [2]. Therefore, the use of different types of fiber-reinforced polymer (FRP) reinforcements in place of steel has gained space, especially in structures located in aggressive environments [3].

FRP rebars are constituted by a tangle of high strength and stiffness fibers impregnated in a low modulus resin, which characterizes them as anisotropic materials. The fibers contribute to the material tensile strength and modulus, whereas the polymeric matrix governs the overall stress-strain relationship and protects the fibers against the concrete environment [4]. Moreover, the resin low modulus entails very large strains, which ensures that the maximum load is transferred to the fibers [5].

FRP is also a lightweight material. Its specific weight varies from 20 to 25% of that of steel, which facilitates the handling process. This property allows using FRP rebars in slender columns, where steel congestion is very common [3]. Moreover, FRP has been utilized as internal reinforcement for tunnels, retaining walls, bridges, highway pavements and sea walls. It also constitutes an economic solution for repairing existing bridges, replacing the conventional steel of the decks [6].

The most popular polymeric rebars are defined according to their respective types of fiber: aramid (AFRP), carbon (CFRP) and glass (GFRP). Among all FRP categories, CFRP has the highest tensile strength and elasticity modulus; however, the raw materials necessary for its production are difficult to find, and the production of carbon fibers requires high energy consumption, which makes the utilization of CFRP very costly [6]. AFRP bars, in turn, are characterized by their high tensile strength and toughness, in addition to possessing the highest strength-to-weight ratio [4].

Nonetheless, losses in strength due to sustained stresses and exposition to UV radiation have limited the AFRP use in the civil construction [5]. In contrast, GFRP became the most popular non-metallic reinforcement due to its low cost and environmental resistance [6]. Some of GFRP properties include excellent response to cyclic loads, high strength-to-weight ratio, non-conductivity and coefficient of thermal expansion close to that of concrete [7].

Despite the corrosion resistance, non-conductivity and lightweight, FRP rebars behave linearly up to failure, not exhibiting a yield plateau as steel does. The cross-sections fail due to either concrete crushing or FRP rupture. Both failure modes are fragile; yet, previous versions of ACI 440.1R-15 [3] recommended over-reinforcing the cross-sections since concrete exhibits some plateau before failure.

2 RESEARCH SIGNIFICANCE

As previously mentioned, the costs with structural repairs have considerably increased, which suggests the gradual replacement of steel by non-metallic reinforcements such as FRP. However, there is no code approaching the design of FRP flexural members, which means the responsibility for structural safety and functionality is entirely attributed to the designer [6]. Furthermore, in spite of the excellent design examples presented by ACI 440.1R-15, this guideline does not address the design of T-shape sections. All examples refer to rectangular sections, with priority to compression-controlled members.

T-shape beams often occur in practice, given the need to consider the slab contribution to the flexural strength. Their design with FRP rebars is not as simple as that of steel, especially for under reinforced cross-sections where the parameters α and λ of the concrete simplified stress block are unknown. There are several design approaches that depend on the neutral axis position associated to FRP and concrete simultaneous failure, as well as that related to the initiation of the concrete non-linear behavior at the most compressed fiber [8].

Therefore, the development of computational programs incorporating the FRP constitutive models and safety factors to a particular reinforced concrete code has the potential to familiarize students and engineers with the design of T-shape beams reinforced with FRP, given the need to replace steel by durable and sustainable materials. Furthermore, they are able to calculate the same cross-section for different FRP types and concrete strength grades, electing the design that combines structural safety and functionality to economic solutions.

3 SCOPE

This paper incorporates the FRP parameters provided by ACI 440.1R-15 [3] to the Brazilian code NBR 6118:2014 [9], deducing the formulations to calculate the FRP longitudinal reinforcement of tension and compression-controlled T-shape sections. The design assumptions accounted for failure due to concrete crushing and FRP rupture, neutral axes on the flange or web and concrete exhibiting linear or non-linear behavior. Additionally, considering that the reinforcement areas

may be adjusted to avoid creep rupture, the assumptions and formulations to compute the final flexural strength are also described. Those formulations are validated by comparing the flexural capacities obtained experimentally to those predicted by the proposed procedures.

The primordial objective was to computationally implement those formulations, developing a design program that calculates the longitudinal FRP reinforcement of T-sections under different scenarios of failure mode, neutral axis position and concrete linear or non-linear behavior. The objective was to identify effective combinations of FRP and concrete strengths resulting in balanced sections, ductility and proper use of materials' mechanical properties. Furthermore, this research aimed to evaluate changes in failure modes, flexural strengths and curvatures caused by adjustments in the FRP areas to avoid creep rupture.

4 DESIGN FOR THE ULTIMATE LIMIT STATE FOR FLEXURE

In order to develop the formulations for the design, the concrete constitutive model of NBR 6118:2014 [9] as well as its parameters were utilized. Figure 1 illustrates the parabola-rectangle model defined by Equations 1 and 2.

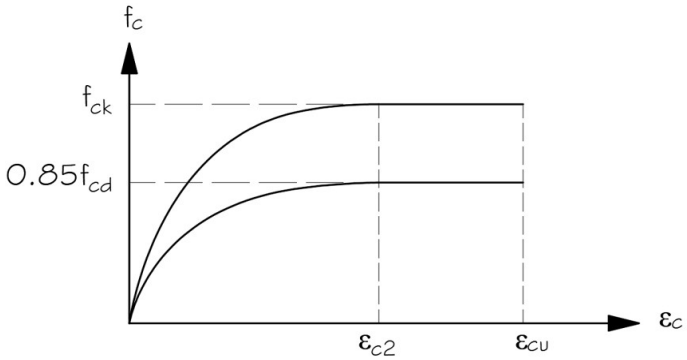

Figure 1. Concrete constitutive model for compression, for which $0.85f_{cd}$ and f_{ck} correspond to the design and characteristic strength, respectively [9]

$$\sigma_{cd} = 0.85f_{cd}\left[1-\left(1-\frac{\varepsilon_c}{\varepsilon_{c2}}\right)^n\right] \text{ if } 0 \leq \varepsilon_c < \varepsilon_{c2} \tag{1}$$

$$\sigma_{cd} = 0.85f_{cd} \text{ if } \varepsilon_{c2} \leq \varepsilon_c < \varepsilon_{cu} \tag{2}$$

The FRP RC cross-sections fail due to concrete crushing or reinforcement rupture. ACI 440.1R-15 [3] introduces the concept of balanced reinforcement ratio, for which both failure modes occur simultaneously. The balanced area A_b is associated to the neutral axis position x_b and to the balanced moment M_b. Unlike ACI 440.1R-15, Barbosa [8] compares the design moment M_d to M_b to define the failure mode. If $M_d < M_b$, the cross-section is tension-controlled, whereas $M_d \geq M_b$ indicates compression-control. Since concrete and FRP reaches their ultimate strains ε_{cu} and ε_{fud} simultaneously, x_b is obtained through compatibility as:

$$x_b = \left(\frac{\varepsilon_{cu}}{\varepsilon_{cu} + \varepsilon_{fud}}\right) d \tag{3}$$

Table 4.2.1 of ACI 440.1R-15 [3] establishes intervals of tensile strengths f_{fu}* and elasticity moduli E_f for the three types of FRP rebars. The strengths are reduced by the environmental coefficients specified in Table 6.2 of this guideline. Unlike NBR 6118:2014 [9], ACI 440.1R-15 imposes safety factors to the cross-section flexural strength and not to the FRP tensile strength. Thus, to incorporate the FRP parameters to NBR 6118:2014 [9] design procedures, the adjusted strength for environmental conditions still needs another factor. As indicated by the Brazilian Recommended Practice for FRP RC structures CT 303 [10], the value of 1.30 was adopted. Thus, the design tensile strength f_{fud} accounts for the environment and eventual uncertainties covered by this factor.

Figures 2 and 3 illustrate balanced sections for which the concrete simplified stress block reaches the flange and web, respectively, resulting in two different approaches to calculate M_b. If $\lambda_u x_b < h_f$, the calculation of the balanced moment accounts only for the flange compressed area. Otherwise, if $\lambda_u x_b \geq h_f$, both flange and web compressed areas are considered. Equations 4 and 5 define the balanced moments for both scenarios, following the order they were mentioned:

$$M_b = \alpha_u \lambda_u f_{cd} b_f x_b (d - 0.5\lambda_u x_b) \quad (4)$$

$$M_b = \alpha_u f_{cd} [\lambda_u x_b b_w (d - 0.5\lambda_u x_b) + h_f (b_f - b_w)(d - 0.5h_f)] \quad (5)$$

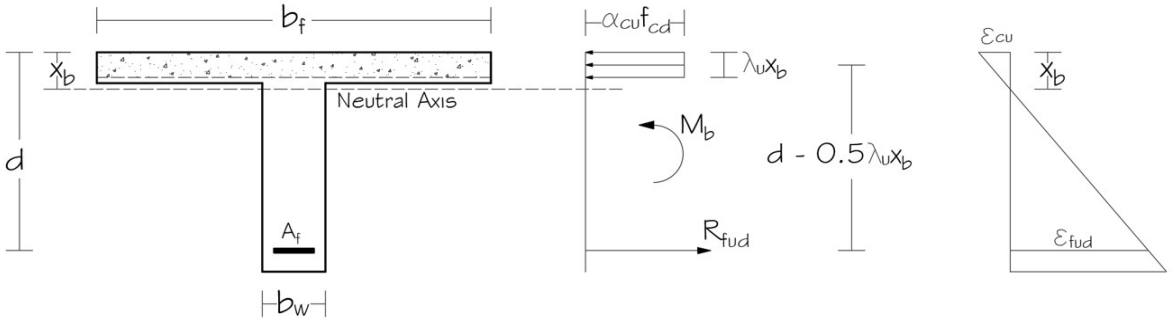

Figure 2. Equilibrium and compatibility of a balanced cross-section with the simplified stress block located on the flange [8]

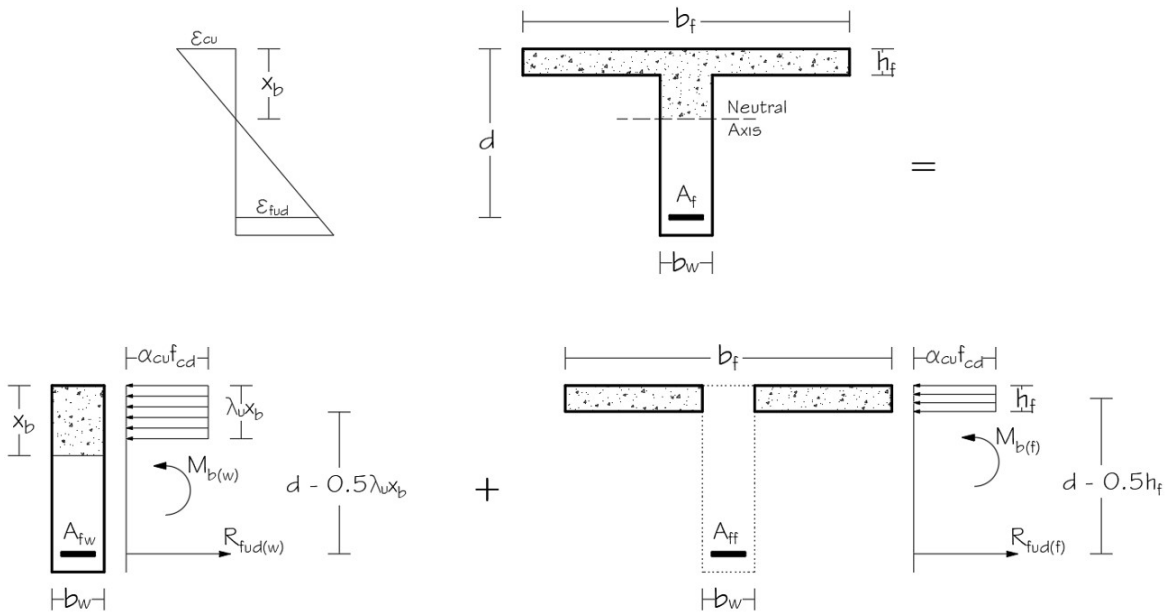

Figure 3. Compatibility and equilibrium of a balanced cross-section with the simplified stress block reaching the web [8]

If the balanced block depth $\lambda_u x_b$ does not reach the web and the design bending moment is lower than the balanced one, the cross-section is tension-controlled and the actual stress block $\lambda_u x$ associated to M_d is smaller than the flange thickness [7]. Moreover, if the cross-section is too under-reinforced, the FRP rebars may fail before the concrete exhibits non-linear behavior. As a result, the values of α_u and λ_u no longer applies, which suggests a linear constitutive model for concrete [3]. Therefore, this scenario results in two design approaches distinguished by the concrete behavior. In contrast, if $M_d \geq M_b$, the actual stress block may reach the web or not, leading to other two approaches [8].

Conversely, if the balanced stress block $\lambda_u x_b$ reaches the web and $M_d < M_b$, there are two possibilities as regards the stress block associated to the design moment: $\lambda_u x < h_f$ or $\lambda_u x \geq h_f$. Furthermore, for each of these two possibilities, concrete may behave linearly or not, resulting in other four design approaches. However, if $M_d \geq M_b$, the actual stress block reaches the web [8]. Therefore, there are nine different design approaches considering only the ultimate limit state for flexure. All formulations are deduced as follows:

4.1 Scenario 1 – Balanced block on the flange and tension-controlled section

This scenario is characterized by $\lambda_u x_b < h_f$ and $M_d < M_b$, which implies that $\lambda_u x < h_f$. However, given the assumption of concrete behaving linearly, it is necessary to define the neutral axis position and the bending moment from which linearity no longer applies. NBR 6118:2014 [9] allows considering the linear stress-strain relationship for stresses under 50% of the concrete compressive strength. Accordingly, this research adopted the maximum stress of $0.5(0.85f_{cd})$, which provides the strain ε_{clin} from Equation 1 as $\varepsilon_{c2}(1\text{-}0.5^{1/n})$. Therefore, the neutral axis x_{lin} related to the linearity limit and obtained through strain compatibility is:

$$x_{lin} = \left(\frac{\varepsilon_{clin}}{\varepsilon_{clin} + \varepsilon_{fud}}\right) d \tag{6}$$

Since the balanced block lies on the flange and the section is tension-controlled, x_{lin} is smaller than the flange thickness [8]. Figure 4 illustrates the equilibrium and compatibility conditions to calculate the moment M_{lin} associated to x_{lin} considering the linear stress-strain relationship for concrete. Thus, if the design moment M_d is lower than the reference moment M_{lin} provided by Equation 7, the linear constitutive model applies [8].

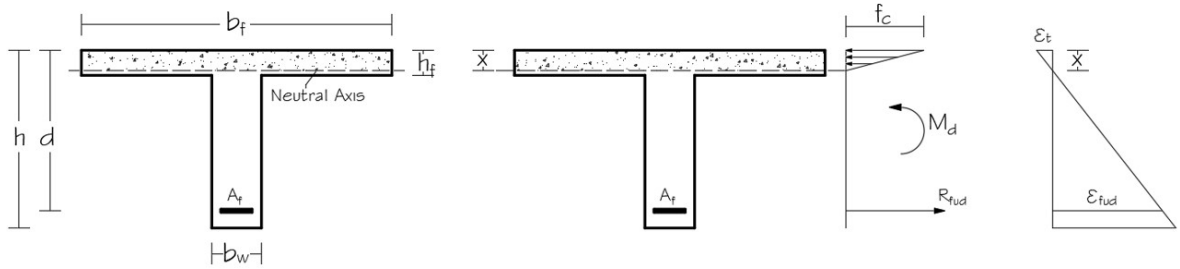

Figure 4. Equilibrium and compatibility conditions of a tension-controlled section with neutral axis on the flange and concrete exhibiting linear behavior [8].

$$M_{lin} = \left(\frac{0.425 f_{cd} x_{lin} b_f}{2}\right)\left(d - \frac{x_{lin}}{3}\right) \tag{7}$$

The secant elasticity modulus E_{lin} adopted for the linear approach corresponds to the slope of the line connecting the origin to the point (ε_{clin}, $0.425f_{cd}$). In order to find the unknown neutral axis depth x, the values of M_{lin} and x_{lin} in Equation 7 are replaced by M_d and x, respectively. The stress $0.425f_{cd}$, in turn, is replaced by the product of the secant modulus E_{lin} and the most compressed fiber strain ε_t, written as a function of x. As a result, there is a cubic equation whose solution within the interval $0 < x < h_f$ corresponds to the neutral axis depth:

$$x^3 - 3dx^2 + \left(\frac{6M_d}{E_{lin}\varepsilon_{fud} b_f}\right)(d - x) = 0 \tag{8}$$

Equation 8 is solved through the Newton-Raphson Method, initially assuming that $x = 1.5x_b$. The iterative process ends once the error $|x_{i+1} - x_i|$ reaches 10^{-5}, which means the neutral axis depth has been found. Negative roots or values exceeding x_{lin} are computationally disregarded. By imposing equilibrium, the required area A_f to resist M_d is found through:

$$A_f = \frac{M_d}{f_{fud}\left(d - \frac{x}{3}\right)} \tag{9}$$

Conversely, if the design moment M_d is higher than M_{lin}, the linear approach no longer applies seeing that the stress in the most compressed fiber exceeds 50% of $0.85f_{cd}$. Although concrete does not fail, ACI 440.1R-15 recommends using, as a conservative approach, the simplified stress block associated to the crushing of the concrete. In this scenario, the parameters α_{cu} and λ_u are calculated as follows, in consonance with NBR 6118:2014 [9]:

$$\alpha_{cu} = 0.85$$

$$\lambda_u = 0.8 \text{ if } f_{ck} \leq 50 \text{ MPa} \tag{10}$$

$$\alpha_{cu} = 0.85[1 - (f_{ck} - 50)/200]$$

$$\lambda_u = 0.8 - (f_{ck} - 50)/400 \text{ if } 50 < f_{ck} \leq 90 \text{ MPa} \tag{11}$$

By imposing the equilibrium conditions illustrated in Figure 5, the neutral axis and the required FRP area are computed as follows:

$$x = \frac{d}{\lambda_u}\left(1 - \sqrt{1 - \frac{2M_d}{\alpha_{cu} f_{cd} b_f d^2}}\right) \tag{12}$$

$$A_f = \frac{M_d}{f_{fud}(d - 0.5\lambda_u x)} \tag{13}$$

Regardless on the concrete behavior, the strain at the most concrete compressed fiber ε_t is computed through compatibility as:

$$\varepsilon_t = \varepsilon_{fud}\left(\frac{x}{d - x}\right) \tag{14}$$

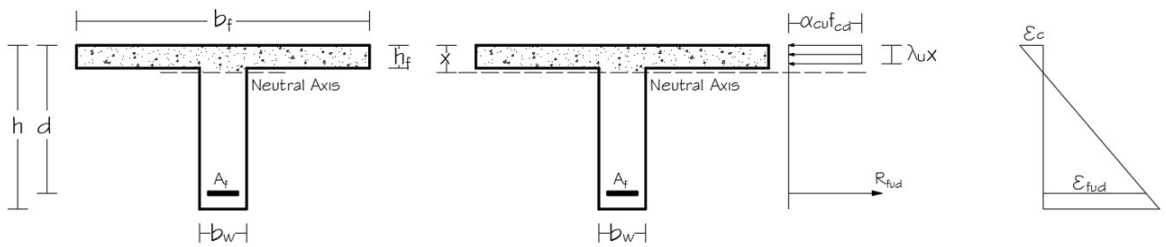

Figure 5. Equilibrium and compatibility conditions of a tension-controlled section for which concrete behaves non-linearly [8].

4.2 Scenario 2 – Balanced block on the web and tension-controlled section

If the balanced stress block reaches the web and the cross-section is tension-controlled, there are four possibilities: first, the actual stress block is on the flange and the concrete linear approach applies; second, the stress block remains on the flange but concrete exhibits non-linear behavior; third, the stress block reaches the web while concrete behaves linearly and fourth, the linear approach no longer applies for the stress block on the web [8].

Furthermore, the reference neutral axis x_{lin} may be either on the flange or web, which results in two different methods to compute the reference moment M_{lin}. If $x_{lin} < h_f$, M_{lin} is determined from Equation 7; otherwise, the compressive stresses on the flange and web must be considered as shown in Figure 6. First, it is necessary to determine the resulting

compressive force F_{lin} from Equation 15 and its center $\bar{y}_{lin}$ from Equation 16. Therefore, the reference moment M_{lin} is computed as the product of F_{lin} and the moment arm d - $\bar{y}_{lin}$.

$$F_{lin} = \frac{1}{2} E_{lin} \varepsilon_{clin} \left[\left(2 - \frac{h_f}{x_{lin}} \right) (b_f - b_w) h_f + b_w x_{lin} \right] \tag{15}$$

$$\bar{y}_{lin} = \frac{\frac{b_w x_{lin}^2}{3} + h_f^2 \left(1 - \frac{2}{3} \frac{h_f}{x_{lin}} \right) (b_f - b_w)}{b_w x_{lin} + h_f \left(2 - \frac{h_f}{x_{lin}} \right) (b_f - b_w)} \tag{16}$$

If $x_{lin} < h_f$ and $M_d < M_{lin}$, the neutral axis x and the reinforcement area A_f are computed through Equations 8 and 9, the same as for scenario 1. Conversely, if $x_{lin} \geq h_f$ and $M_d < M_{lin}$, the neutral axis x associated to M_d may be on the flange or web. Initially, it is assumed that $x < h_f$, for which Equation 8 applies. If the value found for x is smaller than the flange thickness, the assumption is correct, and the required area is computed through Equation 9. Nonetheless, if $x \geq h_f$, the assumption is incorrect, and the value of x is not valid. Consequently, the calculation of the neutral axis depth and the required FRP area must account for the compressive stresses on the flange and web as shown in Figure 6.

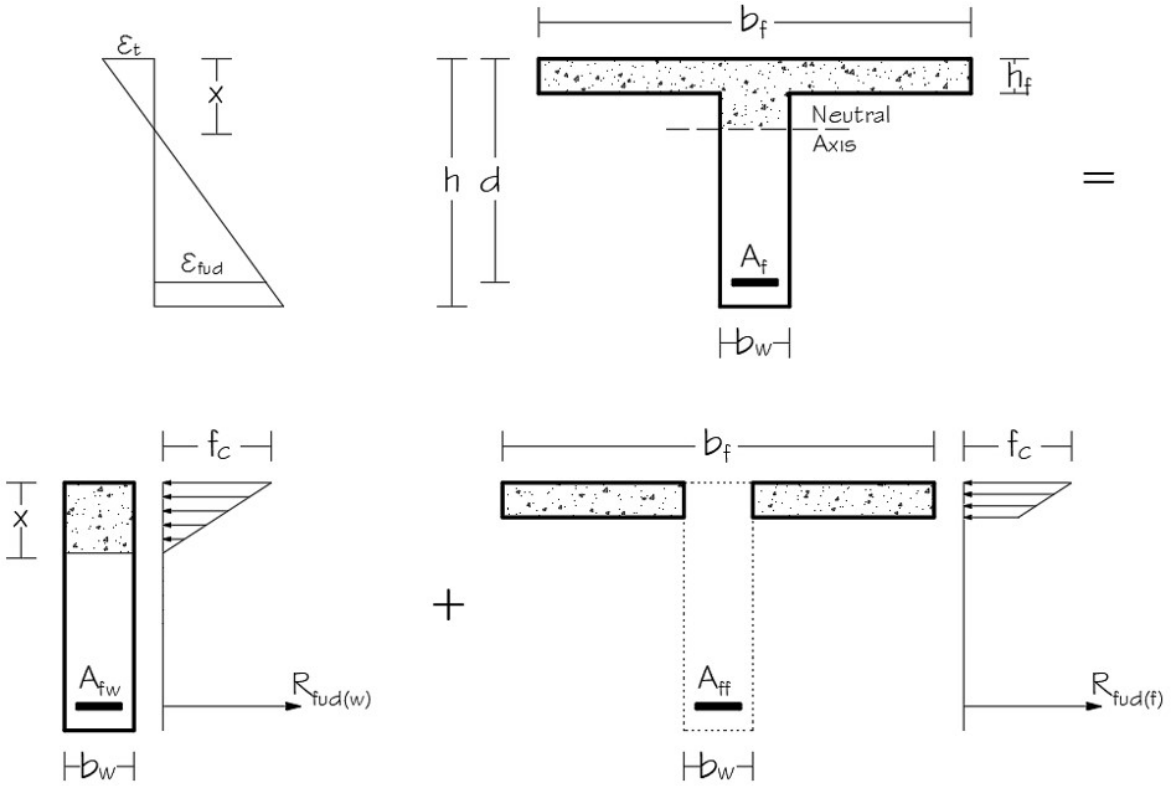

Figure 6. Compatibility and equilibrium of a tension-controlled cross-section for which the concrete linear stress-strain relationship applies [8].

Thus, the variables x_{lin} and ε_{clin} in Equations 15 and 16 are replaced by the neutral axis depth x and the strain at the most compressed fiber ε_t, respectively. Since the strain ε_t can be written as a function of x, the neutral axis depth becomes the only unknown variable. As a result, the expression F_c (d - $\bar{y}_c$) = M_d results in a third-degree equation described as follows:

$$a_1 = \frac{6 h_f (d - 0.5 h_f)(b_f - b_w)}{b_w} \tag{17}$$

$$a_2=\frac{3h_f^2[d - (h_f/3)](b_f - b_w)}{b_w} \quad (18)$$

$$a_3=\frac{6M_d}{E_{lin}\varepsilon_{fud}b_w} \quad (19)$$

$$x^3 - 3dx^2 - (a_1 + a_3)x + (a_3d + a_1h_f - a_2) = 0 \quad (20)$$

Equation 20 is solved exactly as Equation 8, through the Newton-Raphson Method, initially arbitrating x as $1.5x_b$ and ceasing the iterative process once the error becomes smaller than 10^{-3}. Entering the value of x in F_c leads to the resulting compressive and tensile forces, which allows determining the required FRP area as:

$$A_f = \frac{F_c}{f_{fud}} \quad (21)$$

However, if $x_{lin} < h_f$ and $M_d \geq M_{lin}$, concrete behaves non-linearly and the simplified stress block related to M_d may reach either only the flange or the web. First, it is assumed that $\lambda_u x < h_f$ so that x is computed through Equation 12. If the found neutral axis depth is smaller than h_f/λ_u, the assumption is confirmed, and the reinforcement area computed through Equation 13. In contrast, if $x \geq h_f/\lambda_u$, the assumption is incorrect, and the calculation of x needs to account for both flange and web compressed areas.

Figure 7 illustrates the cross-section analysis for two bending moments: M_{dw} and M_{df}, accounting for the areas $b_w x$ and $(b_f - b_w)h_f$, respectively. They are directly determined as:

$$M_{df} = \alpha_{cu}f_{cd}h_f(b_f - b_w)(d - 0.5h_f) \quad (22)$$

$$M_{dw} = M_d - M_{df} \quad (23)$$

Since the neutral axis position relies on the compressed area $b_w x$ and the moment M_{dw}, its depth x is computed as follows:

$$x = \frac{d}{\lambda_u}\left(1 - \sqrt{1 - \frac{2M_{dw}}{\alpha_{cu}f_{cd}b_w d^2}}\right) \quad (24)$$

The areas A_{fw} and A_{ff} illustrated in Figure 7 are calculated to resist the moments M_{dw} and M_{df}, respectively. Thus, the total reinforcement area A_f corresponds to:

$$A_f = \frac{1}{f_{fud}}\left(\frac{M_{dw}}{d - 0.5\lambda_u x} + \frac{M_{df}}{d - 0.5h_f}\right) \quad (25)$$

This approach is also valid if $x_{lin} \geq h_f$ and $M_d \geq M_{lin}$ considering that concrete exhibits non-linear behavior and the stress block $\lambda_u x$ associated to M_d reaches the web. For all these possibilities, the concrete most compressed fiber ε_t is determined in the same manner as for the scenario 1, through Equation 14.

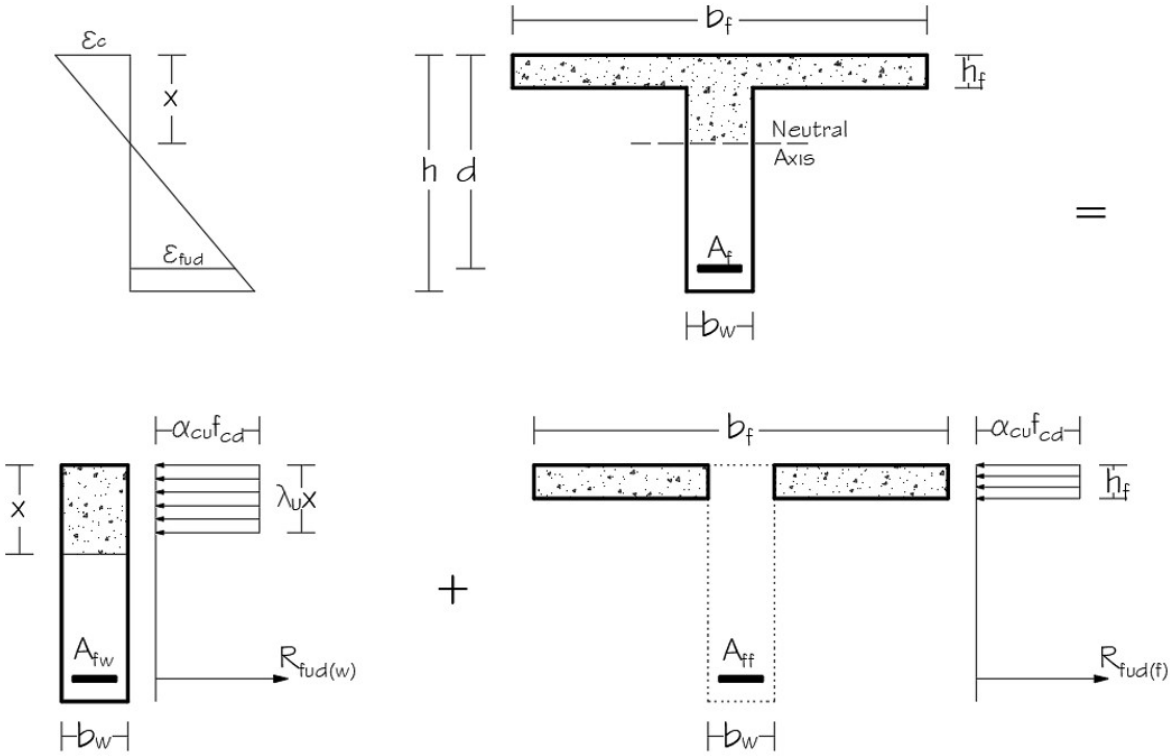

Figure 7. Compatibility and equilibrium of a tension-controlled section for which the concrete behaves non-linearly [8].

4.3 Scenario 3 - Balanced block on the flange and compression-controlled section

If the balanced stress block lies on the flange and the design moment is higher than the balanced one, the cross-section is over-reinforced and the stress block $\lambda_u x$ can reach the web or not. First, it is assumed that $\lambda_u x < h_f$, with x obtained from Equation 12. If the value found for x confirms this assumption, the next step consists of computing the reinforcement stress f_f. Since FRP exhibits linear elastic behavior, the compatibility conditions illustrated in Figure 8 allows determining f_f directly from its strain as:

$$f_f = E_f \varepsilon_{cu} \left(\frac{d - x}{x}\right) \tag{26}$$

The required area A_f found through equilibrium is calculated as follows:

$$A_f = \frac{M_d}{f_f(d - 0.5\lambda_u x)} \tag{27}$$

However, if the neutral axis depth obtained from Equation 12 is equal to or higher than h_f/λ_u, the assumption is incorrect, and the stress block reaches the web. Figure 9 depicts the cross-section analysis for the calculation of the neutral axis depth and reinforcement area.

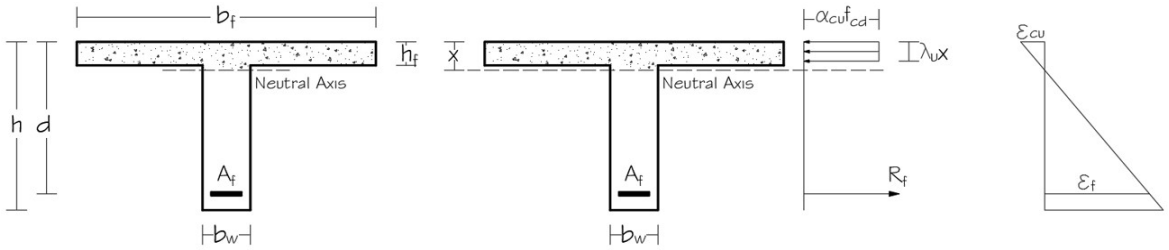

Figure 8. Equilibrium and compatibility of a compression-controlled section with stress block on the flange [8].

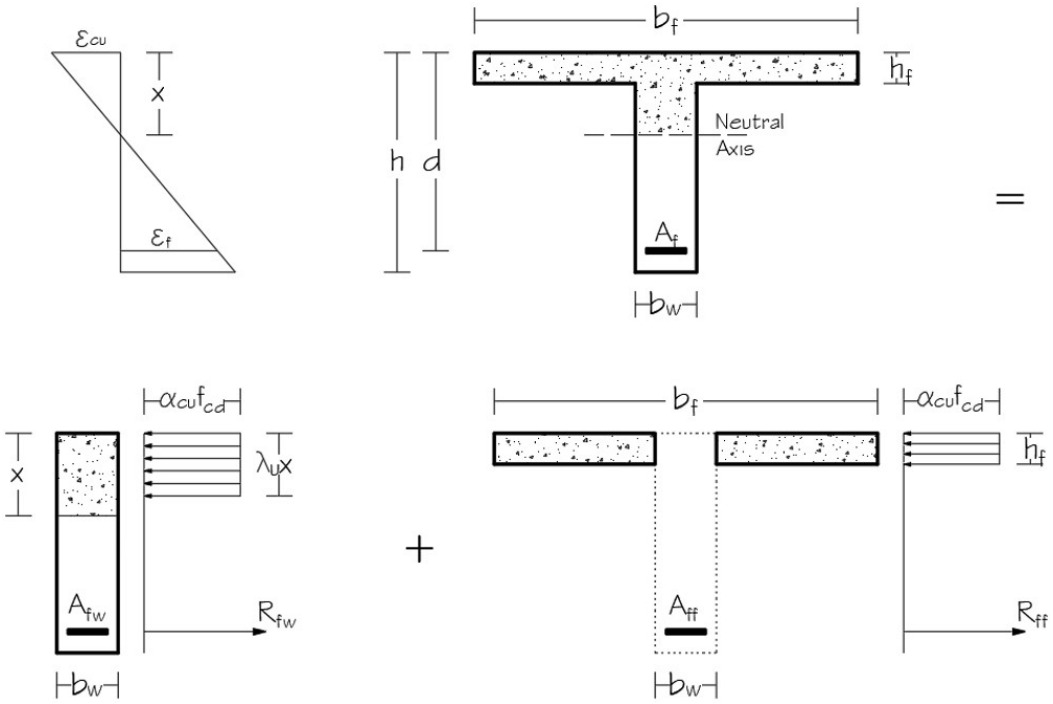

Figure 9. Equilibrium and compatibility of a compression-controlled section whose stress block reaches the web [8].

The moments M_{df}, M_{dw} as well as the neutral axis depth x are obtained from Equations 22, 23 and 24. This approach is the same as that of tension-controlled sections with stress block reaching the web and concrete behaving non-linearly. Nonetheless, the reinforcement stress is not equal to f_{fud} since the FRP rebars do not fail. Therefore, the stress in the FRP layer is obtained from Equation 26, and the total reinforcement area A_f from:

$$A_f = \frac{1}{f_f}\left(\frac{M_{dw}}{d - 0.5\lambda_u x} + \frac{M_{df}}{d - 0.5h_f}\right) \tag{28}$$

4.4 Scenario 4 - Balanced block on the web and compression-controlled section

Unlike the scenario 3, $\lambda_u x_b \geq h_f$ and $M_d \geq M_b$, which ensures that the stress block depth $\lambda_u x$ is equal to or larger than the flange thickness. Therefore, the compatibility and equilibrium conditions for this scenario are also illustrated in Figure 9. The neutral axis depth x and the reinforcement area A_f, in turn, are computed through Equations 24 and 28, respectively.

5 CHECKING FOR FRP CREEP RUPTURE

The required area A_f to meet the ultimate limit state for flexure may not be enough to avoid creep rupture due to sustained stresses [8]. ACI 440.1R-15 establishes that such stresses must not exceed 20, 30 and 55% of the tensile

strength f_{fu} for GFRP, AFRP and CFRP, respectively. Accordingly, the tensile strength f_{fu} for this verification accounts only for the environmental conditions, not incorporating other safety factors.

To determine the sustained stresses f_{fs}, the load combination defined as almost permanent by NBR 6118:2014 [9] was implemented. Additionally, Equations 29 to 31 developed by Ghali and Favre [11] were used to calculate the neutral axis depths x_{cr} under service conditions as shown in Figure 10. The parameter η_f, in turn, refers to the modular ratio E_f / E_{cs}.

$$a_1 = \frac{b_w}{2} \tag{29}$$

$$a_2 = h_f(b_f - b_w) + \eta_f A_f \tag{30}$$

$$a_3 = -d\eta_f A_f - \frac{h_f^2}{2}(b_f - b_w) \tag{31}$$

$$x_{cr} = \frac{-a_2 + \sqrt{a_2^2 - 4a_1 a_3}}{2a_1} \tag{32}$$

The cracking moment of inertia I_{cr} depends on the neutral axis position. Equations 33 and 34 apply for $x_{cr} < h_f$ and $x_{cr} \geq h_f$, respectively [12]. To find the sustained stress f_{fs}, ACI 440.1R-15 and NBR 6118:2014 [9] adopt the linear approach defined in Equation 35. The moment M_{apc} refers to the almost permanent load combination.

$$I_{cr} = \frac{b_f x_{cr}^3}{3} + \eta_f A_f (x_{cr} - d)^2 \tag{33}$$

$$I_{cr} = \frac{(b_f - b_w) h_f^3}{12} + \frac{b_w x_{cr}^3}{3} + (b_f - b_w)\left(x_{cr} - \frac{h_f}{2}\right)^2 + \eta_f A_f (x_{cr} - d)^2 \tag{34}$$

$$f_{fs} = M_{apc}\eta_f \frac{(d - x_{cr})}{I_{cr}} \tag{35}$$

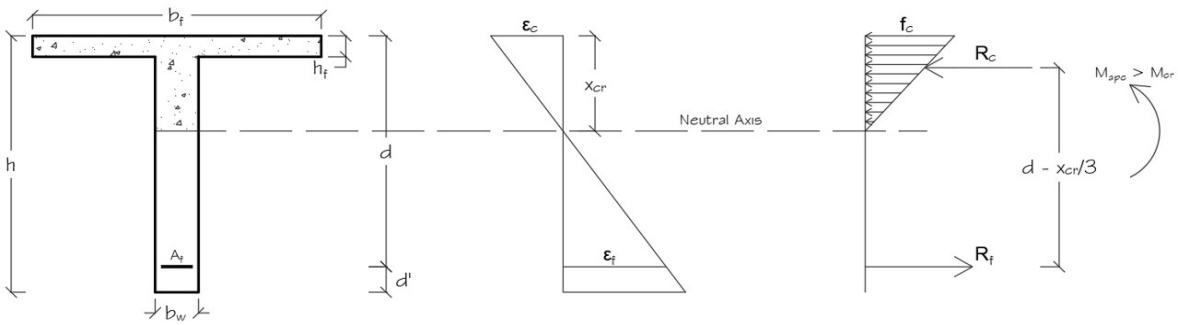

Figure 10. Compatibility and equilibrium to compute the sustained stress considering the almost permanent load combination [12].

If the sustained stress exceeds the maximum allowed by ACI 440.1R-15, areas of 0.001 cm^2 are progressively incremented to A_f, for which Equations 29 to 35 are computationally solved for each adjustment. The sustained stress decreases continuously, and the final adjusted area A_{adj} is that making the sustained stress equal to or slightly lower than the maximum allowed. Thus, the area A_{adj} meets both limit states for flexure and creep rupture.

6 DETERMINATION OF THE FLEXURAL STRENGTH

Because of increments in FRP areas to meet both limit states, the flexural strengths and the neutral axis depths increase. Consequently, the simplified stress block previously located on the flange may reach the web, the failure mode may switch from tension to compression-controlled and for the cross-sections that remain tension-controlled, the concrete linear behavior may no longer apply [8].

In order to determine the failure mode, the adjusted area is compared to the balanced one A_b and, in case of tension-control, A_{adj} is compared to A_{lin}, the area from which the concrete linear approach no longer applies. There are four scenarios as regards the determination of the flexural strength, explained as follows:

6.1 Tension-Control and balanced block on the flange

If $A_{adj} < A_b$, the cross-section is under-reinforced with failure characterized by the FRP rupture. Additionally, if the balanced block depth is smaller than the flange thickness, the stress block associated to the adjusted area $\lambda_u x_{adj}$ does not reach the web. Furthermore, if $A_{adj} < A_{lin}$, the concrete stress-strain relationship can be considered as linear [8].

By imposing equilibrium in Figure 4, the area A_{lin} for which the stress in the most compressed fiber corresponds to 50% of $0.85f_{cd}$ is:

$$A_{lin} = \frac{E_{lin}\varepsilon_{lin}x_{lin}b_f}{2f_{fud}} \tag{36}$$

If $A_{adj} < A_{lin}$, the adjusted neutral axis depth x_{adj} associated to A_{adj} is computed by imposing the equilibrium and compatibility conditions illustrated in Figure 4, which leads to Equations 37 and 38. Once x_{adj} is found, the flexural strength M_r is, thus, obtained from Equation 39.

$$a = \frac{E_{lin}b_f}{2E_f A_{adj}} \tag{37}$$

$$x_{adj} = \frac{\sqrt{1 + 4ad} - 1}{2a} \tag{38}$$

$$M_r = A_{adj}f_{fud}\left(d - x_{adj}/3\right) \tag{39}$$

Conversely, if $A_{adj} \geq A_{lin}$, the simplified stress block represents the concrete constitutive model seeing that the linear approach no longer applies. By imposing the equilibrium conditions shown in Figure 5, the adjusted neutral axis and the flexural strength are determined as follows:

$$x_{adj} = \frac{A_{adj}f_{fud}}{\alpha_{cu}\lambda_u f_{cd}b_f} \tag{40}$$

$$M_r = A_{adj}f_{fud}\left(d - 0.5\lambda_u x_{adj}\right) \tag{41}$$

6.2 Tension-control and balanced block on the web

If $A_{adj} < A_b$ and the balanced stress block reaches the web, the block associated to the adjusted area as well as the reference neutral axis x_{lin} can be located either on the flange or web. If $x_{lin} < h_f$ and $A_{adj} < A_{lin}$, the neutral axis associated to A_{adj} is on the flange [8]. Therefore, the adjusted neutral axis and the flexural strength are obtained from Equations 37, 38 and 39.

However, if $x_{lin} < h_f$ and $A_{adj} \geq A_{lin}$, concrete exhibits non-linear behavior and the adjusted stress block may be located either on the flange or web. First, it is assumed that $\lambda_u x_{adj} < h_f$, which allows computing the adjusted neutral axis and flexural strength through Equations 40 and 41, respectively. However, if the value found for x_{adj} is equal to or higher than h_f/λ_u, the assumption is incorrect; the stress block reaches the web [8]. Therefore, both flange and web compressed areas must be considered. Imposing equilibrium and compatibility for the cross-section illustrated in Figure 7 leads to the correct values of x_{adj} and M_r, computed as follows:

$$x_{adj}=\frac{A_{adj}f_{fud} - \alpha_{cu}f_{cd}h_f(b_f - b_w)}{\alpha_{cu}\lambda_u f_{cd}b_w} \tag{42}$$

$$M_r=\alpha_{cu}f_{cd}\left[\lambda_u b_w x_{adj}\left(d - 0.5\lambda_u x_{adj}\right) + h_f(b_f - b_w)(d - 0.5h_f)\right] \tag{43}$$

In contrast, if $x_{lin} \geq h_f$, Equation 36 no longer applies to compute A_{lin} since the linear distribution of the compressive stresses extends to the web, as shown in Figure 6. Therefore, A_{lin} corresponds to the ratio between F_{lin}, defined in Equation 15, and the FRP design tensile strength f_{fud}. If $A_{adj} < A_{lin}$, the adjusted neutral axis may be on the flange or web. The cross-section analysis illustrated in Figure 4 as well as Equations 37 and 38 determine x_{adj} for the assumption $x_{adj} < h_f$. However, if the solution of such equations provides $x_{adj} \geq h_f$, the assumption is invalid and the correct value of x_{adj} is obtained considering the cross-section analysis shown in Figure 6.

Subsequently, by imposing that the compressive force F_{adj} equals to the ultimate reinforcement load $A_{adj}f_{fud}$, the adjusted neutral axis depth is computed as follows:

$$a_1 = \frac{2}{b_w}\left[(b_f - b_w)h_f + 2A_{adj}\frac{E_f}{E_{lin}}\right] \tag{44}$$

$$a_2 = \frac{1}{b_w}\left[(b_w - b_f)h_f^2 - 2A_{adj}d\frac{E_f}{E_{lin}}\right] \tag{45}$$

$$x_{adj} = a_1\left(\sqrt{\frac{1}{4} - \frac{a_2}{a_1^2}} - \frac{1}{2}\right) \tag{46}$$

The compressive force center $\bar{y}_{adj}$ associated to x_{adj} is obtained from Equation 16, replacing x_{lin} by x_{adj}. Therefore, the adjusted flexural strength corresponds to:

$$M_r = A_{adj}f_{fud}\left(d - \bar{y}_{adj}\right) \tag{47}$$

Finally, if $x_{lin} \geq h_f$ and $A_{adj} \geq A_{lin}$, the stress block associated to A_{adj} reaches the web and the concrete exhibits non-linear behavior. Thus, the adjusted neutral axis depth and the flexural strength are obtained from Equations 42 and 43, according to the cross-section analysis illustrated in Figure 7.

6.3 Compression-control and balanced block on the flange

If the balanced block is located on the flange and the section is compressed-controlled, the stress block associated to A_{adj} may reach the web or not. First, it is assumed that $\lambda_u x_{adj} < h_f$, corresponding to the analysis illustrated in Figure 8. Since the reinforcement does not fail, its strain is unknown, written as a function of x_{adj} [8]. Therefore, since the resulting compression and tension forces are equal, the adjusted neutral axis is obtained as follows:

$$a = \frac{\alpha_{cu}\lambda_u f_{cd}b_f}{E_f\varepsilon_{cu}A_{adj}} \tag{48}$$

$$x_{adj}=\frac{\sqrt{4ad+1}-1}{2a} \tag{49}$$

If the value found for x_{adj} confirms the assumption that $\lambda_u x_{adj} < h_f$, the flexural strength is:

$$M_r = \alpha_{cu}\lambda_u f_{cd}b_f x_{adj}\left(d - 0.5\lambda_u x_{adj}\right) \tag{50}$$

Conversely, if $x_{adj} \geq h_f/\lambda_u$, the assumption is incorrect and Equations 49 and 50 do not apply. It is necessary to consider the compressive stresses on the flange and web as shown in Figure 9, establishing equilibrium of forces and strain compatibility. Thus, x_{adj} is computed as:

$$a_1 = \frac{\alpha_{cu}\lambda_u f_{cd} b_w}{E_f \varepsilon_{cu} A_{adj}} \tag{51}$$

$$a_2 = 1 + \frac{\alpha_{cu} f_{cd} (b_f - b_w) h_f}{E_f \varepsilon_{cu} A_{adj}} \tag{52}$$

$$x_{adj} = \frac{a_2}{a_1}\left(\sqrt{\frac{1}{4} + \frac{a_1}{a_2^2}d} - \frac{1}{2}\right) \tag{53}$$

The flexural strength is obtained from Equation 43, the same as for tension-controlled sections whose neutral axis is on the web and concrete behaves non-linearly [8].

6.4 Compression-control and balanced block on the web

If the balanced block reaches the web and the cross-section is compression-controlled, the adjusted neutral axis depth is larger than the balanced one, which means that $\lambda_u x_{adj} \geq h_f$ as well. Therefore, x_{adj} is computed through Equations 51, 52 and 53 while the flexural strength through Equation 43. The only difference from the previous scenario is that the designer knows for sure that the stress block reaches the web.

7 EXPERIMENTAL VALIDATION

To validate the proposed methodology, the design equations were used to inversely compute the flexural capacities of 125 beams to posteriorly compare with experimental results. The details of all specimens are shown in Table 1, where the reference in brackets indicates the experimental program related to a group of specimens. The T-section dimensions are given as b_w/b_f and h/h_f in the fields corresponding to *b* and *h*, respectively. The abbreviations **TC** and **CC** refer to the tension and compression-controlled failure modes, respectively.

The concrete compressive strengths were obtained experimentally, mostly from testing cylinders in uniaxial compression after 28 days. The majority of experimental programs obtained the FRP mechanical properties from direct tensile tests; others provided only the manufacturer data, as indicated with a * in Table 1. The majority of the beams were tested under four-point bending, with the load applied at a steady rate of 0.8 to 1.2 mm/min or at steps of 2 to 5 kN. Those from [25] and [20], in turn, were tested under three-point loading. All specimens exhibited flexural failure either due to FRP rupture or crushing of the concrete.

Since the experimental flexural capacities are influenced by the actual mechanical properties of materials, the reduction factors for the concrete compressive and FRP tensile strengths were not included in the analytical analysis. The term 0.85 in α_{cu} was also suppressed to account for the short-term loading inherent to the experimental programs. Moreover, since some beams had multiple reinforcement layers, the compatibility and equilibrium equations were adapted to account for different reinforcement distributions. The theoretical and experimental ultimate moments were plotted along with the identity line, and the accuracy of the analytical model assessed through the coefficient of determination R^2.

8 RESULTS AND DISCUSSION

This section addresses two aspects of the results: the experimental validation of the proposed methodology and the application of the design program, considering different examples for each scenario described in Section 4.

8.1 Comparison to Experimental Results

Table 1 summarizes this comparison for each group of beams, considering different concrete grades and FRP types, as well as beams of rectangular and T-sections. The average ratio between theoretical and experimental moments M_{th}/M_{exp} corresponds to 1.0006, with mean deviation of 0.10 and coefficient of determination $R^2 = 0.962$, which suggests agreement of the analytical methods with respect to experimental results. Figure 11 illustrates the scattering of the data in relation to the identity line.

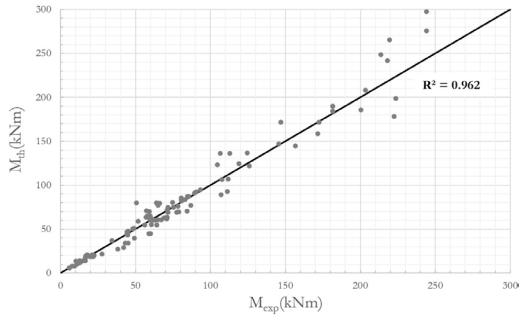

Figure 11 – Correlation scatter plot for the experimental $M_{exp.}$ and theoretical M_{th} flexural capacities

8.2 Program Interface

Using the developed design program, Figure 12 illustrates the calculation of a T-shape section reinforced with AFRP rebars. The user chooses the FRP type and inserts its mechanical properties. Yet, they are not able to define tensile strengths and elasticity moduli out of the intervals defined by Table 4.2.1 of ACI 440.1R-15 for each FRP type. For this example, in particular, the design bending moment corresponds to 98% of the balanced one, which indicates proper use of AFRP and concrete mechanical properties. Nonetheless, since the sustained stress due to the almost permanent load combination is higher than the maximum allowed by ACI 440.1R-15, the required area was increased by 1% to avoid creep rupture. This increment in the FRP area was not enough to switch the failure mode from tension to compression-controlled, resulting in a flexural strength 0.8% higher. This slight increase was not enough to characterize waste of the AFRP rebars' mechanical properties.

If a high-performance concrete with f_{ck} = 90 MPa is used, the cross-section becomes too under-reinforced, with flexural strength corresponding to 38% of the balanced moment. As a result, there is waste of the concrete's mechanical properties since the strain at the top corresponds to only 29% of the ultimate strain ε_{cu}. In conclusion, the grade that best fits the reinforcement type for this particular load condition is the grade C20, which allows taking advantage of both concrete and FRP mechanical properties.

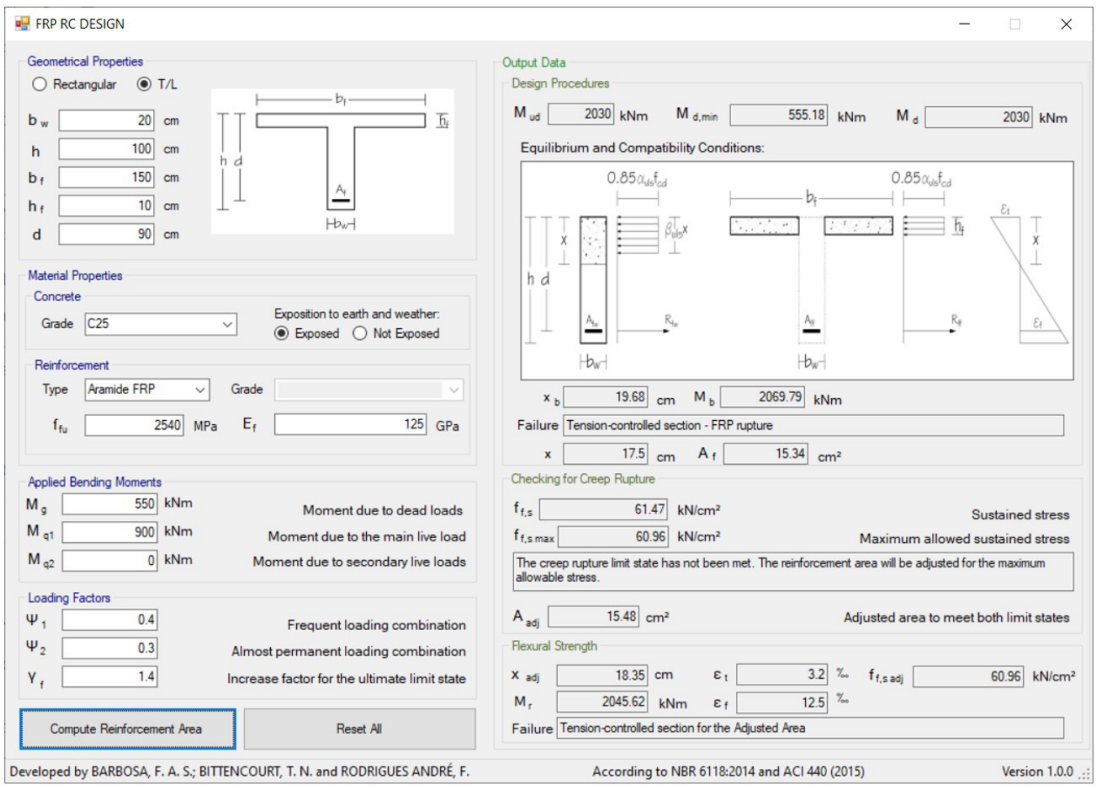

Figure 12. Computation of the AFRP reinforcement area using the developed design program.

Table 1 - Comparison between experimental and predicted flexural capacities

Ref.	Beam	Geometrical features			Materials (MPa)			Ultimate Moments (kNm)			Failure
		b (cm)	h(cm)	ρ_f (%)	f'_c	f_{fu}	10^{-3} E_f	M_{exp}	M_{th}	M_{th}/M_{exp}	
[13]	C1-4	20	30	0.47	40.4	1368.0	114.0	71.20	71.72	1.01	TC
	C1-4b	20	30	0.47	40.4	1368.0	114.0	74.58	80.20	1.08	CC
	C1-6	20	30	0.71	39.3	1368.0	114.0	83.13	83.53	1.00	CC
	C1-8	20	30	0.95	39.3	1368.0	114.0	90.39	92.43	1.02	CC
	C2-4	20	30	0.43	39.9	1904.0	112.0	78.75	69.38	0.88	CC
	C2-4b	20	30	0.43	39.9	1904.0	112.0	78.18	76.16	0.97	CC
	C2-6	20	30	0.64	40.8	1904.0	112.0	80.89	82.09	1.01	CC
	C2-8	20	30	0.85	40.8	1904.0	112.0	89.39	91.09	1.02	CC
	G1-6	20	30	1.29	39.1	600.0	40.0	77.47	68.86	0.89	CC
	G1-8	20	30	1.72	39.1	600.0	40.0	86.76	76.77	0.88	CC
	G2-6	20	30	1.13	39.1	648.0	36.0	71.00	63.03	0.89	CC
	G2-8	20	30	1.51	39.1	648.0	36.0	84.54	70.52	0.83	CC
	AR-6	20	30	0.71	39.1	1716.0	52.0	70.85	61.62	0.87	CC
	AR-8	20	30	0.95	39.1	1716.0	52.0	71.75	69.04	0.96	CC
[14]	BC4NA	13	18	2.03	46.2	772.9	38.0	22.40	20.13	0.90	CC
	BC4NB	13	18	2.03	46.2	772.9	38.0	20.60	20.13	0.98	CC
	BC4HA	13	18	2.03	53.9	772.9	38.0	21.00	20.63	0.98	CC
	BC4HB	13	18	2.03	53.9	772.9	38.0	21.40	20.63	0.96	CC
	BC2NA	13	18	1.02	53.1	772.9	38.0	21.90	18.89	0.86	CC
	BC2NB	13	18	1.02	53.1	772.9	38.0	20.00	18.89	0.94	CC
	BC2HA	13	18	1.02	57.2	772.9	38.0	19.70	18.48	0.94	CC
	BC4HB	13	18	1.02	57.2	772.9	38.0	20.60	18.48	0.90	CC
[15]	CB2B-1	20	30	0.58	52.0	779.0	38.0	57.90	65.04	1.12	TC
	CB2B-2	20	30	0.58	52.0	779.0	38.0	59.80	65.04	1.09	TC
	CB3B-1	20	30	0.87	52.0	779.0	38.0	66.00	79.30	1.20	CC
	CB3B-2	20	30	0.87	52.0	779.0	38.0	64.80	79.30	1.22	CC
	CB4B-1	20	30	1.16	45.0	779.0	38.0	75.40	74.63	0.99	CC
	CB4B-2	20	30	1.16	45.0	779.0	38.0	71.70	74.63	1.04	CC
	CB6B-1	20	30	1.74	45.0	779.0	38.0	84.80	87.48	1.03	CC
	CB6B-2	20	30	1.74	45.0	779.0	38.0	85.40	87.48	1.02	CC
[16]	FB-2	30	40	0.22	30.0	690.0	41.0	68.94	62.75	0.91	TC
	FB-3	30	40	0.33	30.0	690.0	41.0	111.18	93.04	0.84	TC
	FB-4	30	40	0.44	30.0	690.0	41.0	125.88	121.91	0.97	TC
	FB-6	30	40	0.66	30.0	690.0	41.0	171.54	158.56	0.92	CC
	FB-8	30	40	0.88	30.0	690.0	41.0	222.60	178.05	0.80	CC
	HFB-3	30	40	0.33	50.0	690.0	41.0	93.24	94.89	1.02	TC
	HFB-4	30	40	0.44	50.0	690.0	41.0	119.04	124.63	1.05	TC
	HFB-6	30	40	0.66	60.0	690.2	41.0	200.46	185.69	0.93	TC
	HFB-8	30	40	0.88	50.0	690.0	41.0	218.04	241.47	1.11	TC
	HFB-10	30	40	1.11	50.0	690.0	41.0	219.36	265.55	1.21	CC
[17]*	ISO30-2	20	30	0.95	44.0	688.8	42.0	80.40	85.18	1.06	CC
	KD30-1	20	30	0.95	44.0	640.9	49.0	50.60	79.79	1.58	CC
	KD30-2	20	30	0.95	44.0	640.9	49.0	63.80	79.79	1.25	CC
	KD45-1	20	45	0.64	55.0	640.9	49.0	106.60	136.16	1.28	TC
	KD45-2	20	45	0.64	55.0	640.9	49.0	113.00	136.16	1.20	TC
	ISO55-1	20	55	0.52	43.0	688.8	42.0	181.50	184.17	1.01	TC
	ISO55-2	20	55	0.52	43.0	688.8	42.0	181.50	184.17	1.01	TC
	KD55-1	20	55	0.52	43.0	640.9	49.0	146.90	171.48	1.17	TC
	KD55-2	20	55	0.52	43.0	640.9	49.0	172.50	171.48	0.99	TC
[18]*	ISO2	20	30	0.95	43.0	688.5	45.0	80.40	83.26	1.04	CC
	ISO3	20	55	0.52	43.0	688.5	45.0	181.70	189.95	1.05	TC
	ISO4	20	55	0.52	43.0	688.5	45.0	181.70	189.95	1.05	TC
[19]	Beam 2	15	20	0.19	27.7	650.0	38.0	5.89	5.84	0.99	TC
	Beam 4	15	25	0.15	27.7	650.0	38.0	7.85	7.94	1.01	TC
	Beam 6	15	30	0.13	27.7	650.0	38.0	10.79	9.77	0.91	TC
	Beam 8	15	20	0.19	50.1	650.0	38.0	5.89	5.90	1.00	TC
	Beam 10	15	25	0.15	50.1	650.0	38.0	9.48	8.00	0.84	TC
	Beam 12	15	30	0.25	50.1	650.0	38.0	16.75	19.46	1.16	TC

Table 1 – Continued…

Ref.	Beam	Geometrical features			Materials (MPa)			Ultimate Moments (kNm)			Failure
		b (cm)	h(cm)	ρ_f (%)	f'_c	f_{fu}	10^{-3} E_f	M_{exp}	M_{th}	M_{th}/M_{exp}	
[20]*	1FRP1	38 .1	20.3	0.10	27.6	829.7	41.4	11.49	11.60	1.01	TC
	1FRP2	38.1	20.3	0.10	27.6	829.7	41.4	12.67	11.60	0.92	TC
	1FRP3	38.1	20.3	0.10	27.6	829.7	41.4	11.49	11.60	1.01	TC
	2FRP1	31.8	21.6	0.12	27.6	829.7	41.4	13.62	12.46	0.91	TC
	2FRP2	31.8	21.6	0.12	27.6	829.7	41.4	13.26	12.46	0.94	TC
	2FRP3	31.8	21.6	0.12	27.6	829.7	41.4	13.06	12.46	0.95	TC
	4FRP1	20.3	15.2	1.04	27.6	829.7	41.4	15.78	14.68	0.93	TC
	4FRP2	20.3	15.2	1.04	27.6	829.7	41.4	15.58	14.68	0.94	TC
	4FRP3	20.3	15.2	1.04	27.6	829.7	41.4	16.29	14.68	0.90	TC
	5FRP1	19.1	15.2	1.10	27.6	829.7	41.4	16.37	14.14	0.86	CC
	5FRP2	19.1	15.2	1.10	27.6	829.7	41.4	16.65	14.14	0.85	CC
	5FRP3	19.1	15.2	1.10	27.6	829.7	41.4	15.78	14.14	0.90	CC
[21]	C-S-1	20	30	0.75	26.9	1000.0	200.0	64.11	54.50	0.85	TC
	C-S-2	20	30	0.29	27.5	2000.0	200.0	44.28	43.68	0.99	TC
	C-C-3	20	30	0.52	23.6	2000.0	200.0	44.76	43.30	0.97	TC
	C-C-4	20	30	0.52	27.2	1000.0	200.0	60.66	54.87	0.90	TC
	C-C-5	20	30	0.75	28.0	1000.0	200.0	56.03	54.64	0.98	TC
[22]	T/C150-2	20/70	70/15	0.36	37.5	1060.0	200.0	64.89	76.77	1.18	TC
	T/C150-4	20/70	70/15	0.52	37.5	1060.0	200.0	145.69	146.89	1.01	TC
	T/C100-4	20/70	70/10	0.63	37.5	1060.0	200.0	104.63	123.23	1.18	TC
	R/C-2	20	35	0.47	40.5	1060.0	200.0	57.33	71.05	1.24	TC
	R/C-4	20	35	0.79	40.5	1060.0	200.0	124.60	136.60	1.10	TC
[23]	II	20	21	2.70	31.3	700.0	35.6	34.19	36.84	1.08	CC
	III	20	26	0.98	31.3	886.0	43.4	45.13	47.67	1.06	CC
	IV	20	30	0.95	40.7	700.0	35.6	59.19	69.84	1.18	CC
	V	20	25	2.27	40.7	700.0	35.6	57.00	63.54	1.11	CC
[24]	C-212-D1	14	19	0.85	59.8	1353.0	63.3	38.20	27.13	0.71	CC
	C-216-D1	14	19	1.51	56.3	995.0	64.2	45.06	34.09	0.76	CC
	C-316-D1	14	19	2.27	55.2	995.0	64.2	49.38	39.75	0.80	CC
	C-212-D2	16	19	0.74	39.6	1353.0	63.3	27.69	21.64	0.78	CC
	C-216-D2	16	19	1.32	61.7	995.0	64.2	42.15	29.17	0.69	CC
	C-316-D2	16	19	1.98	60.1	995.0	64.2	43.20	34.07	0.79	CC
[25]	GS1	20	30	1.65	28.0	736.0	46.0	60.20	62.59	1.04	CC
	GS2	20	30	1.65	26.0	736.0	46.0	49.00	50.70	1.03	CC
	CS1	20	30	0.59	26.0	1392.0	116.0	51.80	58.99	1.14	CC
[26]*	B4	15.24	15.24	0.27	51.7	1899.9	140.0	12.60	13.84	1.10	TC
	B5	15.24	15.24	0.27	48.0	1899.9	140.0	10.15	13.76	1.36	TC
	B6	15.24	15.24	0.27	45.9	1899.9	140.0	12.87	13.73	1.07	TC
	B7	15.24	15.24	0.43	49.3	1899.9	140.0	17.10	18.49	1.08	CC
	B8	15.24	15.24	0.43	51.1	1899.9	140.0	16.92	18.45	1.09	CC
	B9	15.24	15.24	0.43	53.3	1899.9	140.0	16.58	18.21	1.10	CC
	B10	15.24	15.24	0.61	53.4	1899.9	140.0	17.85	20.74	1.16	CC
	B11	15.24	15.24	0.61	55.0	1899.9	140.0	17.61	20.59	1.17	CC
	B12	15.24	15.24	0.61	43.9	1899.9	140.0	17.51	19.52	1.12	CC
[27]	AF2T1	15	30	0.35	42.8	1759.6	53.0	44.17	46.58	1.05	CC
	BF3T1	15	30	0.52	85.8	1759.6	53.0	59.46	60.81	1.02	CC
	CF3T1	15	30	0.52	85.6	1759.6	53.0	67.21	60.75	0.90	CC
	DF2T1	15	30	0.35	84.5	1759.6	53.0	48.06	50.28	1.05	CC
	DF3T1	15	30	0.52	84.5	1759.6	53.0	62.77	60.40	0.96	CC
	DF4T1	15	30	0.70	84.5	1759.6	53.0	60.02	62.06	1.03	CC
	DF3T2	15	30	0.52	84.5	1759.6	53.0	62.41	60.40	0.97	CC
	DF3T3	15	30	0.52	84.5	1759.6	53.0	60.80	60.40	0.99	CC
	DS4T2	15	30	1.79	84.5	1759.6	53.0	107.20	89.01	0.83	CC
[28]*	B1T1	15/91	46/7.6	1.07	38.6	620.0	40.0	111.85	106.63	0.95	TC
	B2T1	15/76	46/7.6	1.17	35.2	620.0	40.0	107.79	106.58	0.99	TC
	B3C1	15/46	45/6.4	4.31	21.4	620.0	40.0	203.37	208.13	1.02	CC
	B4T1	15/107	45/6.4	1.27	18.6	620.0	40.0	156.60	144.44	0.92	TC
	B3C2	15/61	37/6.4	3.73	21.4	620.0	40.0	223.71	198.51	0.89	CC
	B1T2	15/91	38/7.6	1.83	38.6	620.0	40.0	213.54	248.59	1.16	TC
	B2C1	15/76	38/7.6	2.57	35.2	620.0	40.0	244.05	297.66	1.22	CC
	B4C1	15/107	37/6.4	3.31	18.6	620.0	40.0	244.05	275.70	1.13	CC

Table 1 – Continued…

Ref.	Beam	Geometrical features			Materials (MPa)			Ultimate Moments (kNm)			Failure
		b (cm)	h(cm)	ρ_f (%)	f'_c	f_{fu}	10^{-3} E_f	M_{exp}	M_{th}	M_{th}/M_{exp}	
[29]	GB1-1	18	30	0.47	35.0	695.0	40.0	60.00	44.82	0.75	TC
	GB1-2	18	30	0.47	35.0	695.0	40.0	59.00	44.82	0.76	TC
	GB2-1	18	30	0.71	35.0	695.0	40.0	65.00	60.69	0.93	CC
	GB2-2	18	30	0.71	35.0	695.0	40.0	64.30	60.69	0.94	CC
	GB3-1	18	30	0.94	35.0	695.0	40.0	71.00	63.27	0.89	CC
	GB3-2	18	30	0.94	35.0	695.0	40.0	70.50	63.27	0.90	CC

*Direct tensile tests not performed by the authors, FRP properties provided by the manufacturer, TC = Tension-controlled; CC = Compression-controlled

8.3 Examples considering different design scenarios

Since there are several approaches to compute the required FRP area, Table 2 describes the design of the same T-shape section illustrated in Figure 12, considering all the possibilities presented in Section 4. The approach 1A and 1B refer to the first scenario, considering the concrete linear and non-linear behavior, respectively. In turn, 2A indicates concrete linearity and $x < h_f$, whereas 2B, non-linearity. Additionally, both 2C and 2D refer to $x \geq h_f$ with concrete behaving linear and non-linear, respectively. Regarding the third scenario, the approaches 3A and 3B refer to $\lambda_u x < h_f$ and $\lambda_u x \geq h_f$, respectively; whereas the only possibility for the fourth scenario, 4A, corresponds to $\lambda_u x_b \geq h_f$ and $M_d \geq M_b$.

Table 2. Definition of the failure mode corresponding to all design approaches previously described

Case	FRP	f_{fu}* (MPa)	Exposition	E_f (GPa)	f_{ck} (MPa)	M_d (kNm)	x_b (cm)	M_b (kNm)	Failure Mode
1A	Aramid	2540	No	125	80	2100	14.1	5276.5	TC
1B	Carbon	3690	No	150	60	1820	11.9	4088.2	TC
2A	Glass	683	Yes	51	65	962.7	24.8	5144.1	TC
2B	Glass	600	No	51	40	759.4	29.3	3575.6	TC
2C	Carbon	1300	Yes	145	90	1820	26.6	6142.7	TC
2D	Aramid	2300	Yes	100	20	1582	17.8	1629.0	TC
3A	Carbon	3000	No	120	80	4340	10.7	4149.0	CC
3B	Carbon	3690	Yes	180	90	5670	13.9	5444.6	CC
4A	Aramid	1800	Yes	70	20	1820	16.3	1606.2	CC

Regarding the cases 1A and 1B, the results showed that the balanced block is located on the flange when high-performance concretes are used in conjunction with FRP rebars exhibiting large ultimate strains. If the cross-section is tension-controlled, the concrete linear stress-strain relationship is more likely to apply if the applied bending moment is considerably lower than the balanced one, especially if high-performance concretes are used.

In contrast, the second scenario is characterized by the use of FRP with low deformability compared to first scenario. As a result, the balanced block reached the web. However, since the design bending moments regarding 2A and 2B are significantly lower than the balanced ones, their respective stress blocks fell on the flange. Even though the design moments corresponding to 2C and 2D are lower than the balanced ones, their respective neutral axes are positioned on the web. However, the linear approach applied only for 2B.

Alike the possibilities 1A and 1B, the association of high-performance concretes with large deformability FRP caused the balanced block to reach only the flange for cases 3A and 3B. In contrast, the applied moments are higher than the balanced ones, making stresses blocks fall on the flange and web, respectively. Regarding 4A, the association of concrete and FRP is similar to that of scenario 2, with the balanced block reaching the web.

The design for the ultimate limit state and verification for creep rupture are described in Table 3. The adjustments in AFRP and GFRP areas for 1A, 2A and 2B resulted in deeper neutral axes x_{adj} and increased top concrete strains ε_c, not reducing the reinforcement strains ε_f. As a result, the cross-section curvatures φ slightly increased, improving ductility. The CFRP RC compression-controlled sections 3A and 3B, in turn, exhibited the largest curvatures while the tension-controlled 2C, the smallest.

Since the cross-sections 2A, 2B and 2C are tensile-controlled with small curvatures, the designer may either increase the amount of reinforcement up to the balanced area A_b or decrease the compressive strength f_{ck}, which would lead to larger curvatures. However, if the section becomes compression-controlled, a further increase in A_f or decrease in f_{ck} would deepen the neutral axis and reduce the FRP strain, leading to smaller curvatures.

Table 3. Design for the ultimate limit state and checking for creep rupture for all approaches

Case	x (cm)	A_f (cm^2)	M_{apc} (kNm)	f_{fs} (MPa)	A_{adj} (cm^2)	A_b (cm^2)	Failure	x_{adj} (cm)	ε_c (‰)	ε_f (‰)	M_r (kNm)	$10^3\varphi$ (rad/m)
1A	5.3	13.0	1010	841.4	16.7	35.3	TC	6.8	1.10	14.1	2678.3	0.17
1B	5.1	7.3	810	1244	7.3	16.9	TC	5.1	1.15	18.9	1820.0	0.22
2A	8.6	30.0	325	122	38.7	166.5	TC	9.7	0.87	7.21	1233.4	0.09
2B	2.9	23.2	360	175.5	43	116.4	TC	5.5	0.47	7.24	1394.4	0.09
2C	11.6	23.5	880	431	23.5	81.2	TC	11.6	0.92	6.21	1820.0	0.08
2D	14.7	13.2	549	477	13.2	13.6	TC	14.7	2.76	14.15	1582.0	0.19
3A	11.3	23.1	1700	841.9	23.1	20.9	CC	11.3	2.60	18.22	4340.0	0.23
3B	16.3	31.5	3350	1307.4	31.5	25.0	CC	16.3	2.6	11.78	5670.0	0.16
4A	31.9	49.2	1090	279	49.2	17.1	CC	31.9	3.5	6.39	1820.0	0.11

9 CONCLUSIONS

This paper implemented the FRP mechanical properties provided by ACI 440.1R-15 [3] to the Brazilian code NBR 6118:2014 [9], developing the equations for the design of T-shape sections reinforced by FRP rebars. The deduced formulations accounted for all possibilities of neutral axis position, failure mode and concrete behavior, which resulted in a design applet that calculates the FRP area based on the ultimate limit state for flexure and creep rupture.

The design procedures were validated by comparing the predicted flexural capacities with experimental results available in the literature for 125 beams. The average ratio between computed and experimental ultimate moments corresponds to 1.0006 with mean deviation of 0.10 and R^2 = 0.962, which suggests efficacy of the proposed methodology to compute the required amount of flexural FRP reinforcement given a design bending moment.

In conclusion, since there is no guideline deeply addressing the design of T-shape beams reinforced by FRP rebars, the presented design approaches can help students and engineers to understand how these members behave, considering different combinations of FRP and concrete grades. Therefore, they are able to elect the ones that provide the best results in terms of ductility, flexural strength and economical solutions.

ACKNOWLEDGEMENTS

This study was financed by the Coordination for the Improvement of Higher Education Personnel - Brazil (CAPES) - Finance Code 001 and Catedra Under Rail – VALE.

REFERENCES

[1] A. M. Neville, "Consideration of durability of concrete structures: past, present and future," *Mater. Struct.*, vol. 34, pp. 114–118, 2001.

[2] L. Bertolini, "Steel corrosion and service life of reinforced concrete structures," *Struct. Infrastruct. Eng.*, vol. 4, no. 2, pp. 123–137, 2008.

[3] American Concrete Institute, *Guide for the Design and Construction of Structural Concrete Reinforced with Fiber-Reinforced Polymer (FRP) Bars*, ACI 440.1R-15, 2015, 83 p.

[4] *fib* International Federation for Structural Concrete, *FRP Reinforcement in RC Structures* (Bulletin 40). Lausanne: *fib* Task-Group 9.3, Federal Institute of Technology, 2007, 147 p.

[5] C. Tuakta, “Use of fiber-reinforced polymer composite in bridge structures,” M.S. thesis, Massachusetts Inst. Technol., Cambridge, 2005, 50 p.

[6] E. Gudonis, E. Timinskas, V. Gribniak, G. Kaklauskas, A. K. Arnautov, and V. Tamulènas, "FRP reinforcement for concrete structures: state-of-the-art review of application and design," *Eng. Struct. Technol.*, vol. 5, no. 4, pp. 147–158, 2013.

[7] D. H. Tavares, J. S. Giongo, and P. Paultre, "Behavior of reinforced concrete beams reinforced with GFRP bars," *Ibracon Struct. Mater. J.*, vol. 1, no. 3, pp. 285–295, 2008.

[8] F. A. S. Barbosa, “Numerical assessment of concrete flexural members reinforced by FRP rebars,” M.S. thesis, Univ. São Paulo, São Paulo, 2020.

[9] Associação Brasileira de Normas Técnicas, *Projeto de Estruturas de Concreto,* ABNT NBR 6118, 3ª ed., 2014, 238 p.

[10] Comitê IBRACON/ABECE, *Prática Recomendada CT 303 – Estruturas de Concreto Armado com Barras de Polímero Reforçado com Fibras (FRP)*, 1ª ed. São Paulo: IBRACON, 2021, 63 p.

[11] A. Ghali and R. Favre, *Concrete Structures: Stresses and Deformations*, 1st ed. London, UK: Chapman & Hall, 1986, 352 p.

[12] R. C. Carvalho and J. R. Figueiredo Fo., *Cálculo e Detalhamento de Estruturas Usuais de Concreto Armado: Segundo a NBR 6118:2014*, 4ª ed. São Carlos: Edufscar, 2014, 415 p.

[13] C. Kassem, A. S. Farghaly, and B. Benmokrane, "Evaluation of flexural behavior and serviceability performance of concrete beams reinforced with FRP bars," *J. Compos. Constr.*, vol. 5, no. 11, pp. 682–695, 2011.

[14] M. Thériault and B. Benmokrane, "Effects of FRP reinforcement ratio and concrete strength on flexural behavior of concrete beams," *J. Compos. Constr.*, vol. 2, no. 1, pp. 7–16, 1998.

[15] R. Masmoudi, M. Thériault, and B. Benmokrane, "Flexural behavior of concrete beams reinforced with deformed fiber reinforced plastic reinforcing rods," *ACI Struct. J.*, vol. 5, no. 6, pp. 665–675, 1998.

[16] Ridwan and D. T. Putri, "Flexural capacity of concrete beam reinforced with GFRP bars," *J. Phys. Conf. Ser.*, vol. 2049, no. 1, pp. 012075, 2021.

[17] B. Benmokrane, O. Chaallal, and R. Masmoudi, "Glass Fibre Reinforced Plastic (GFRP) rebars for concrete structures," *Constr. Build. Mater.*, vol. 9, no. 6, pp. 353–364, 1995.

[18] B. Benmokrane, O. Chaallal, and R. Masmoudi, "Flexural response of concrete beams reinforced with FRP reinforcing bars," *ACI Struct. J.*, vol. 91, no. 2, pp. 46–55, 1996.

[19] A. F. Ashour, "Flexural and shear capacities of concrete beams reinforced with GFRP bars," *Constr. Build. Mater.*, vol. 20, pp. 1005–1015, 2006.

[20] J. R. Yost, C. H. Goodspeed, and E. R. Schmeckpeper, "Flexural performance of concrete beams reinforced with FRP grids," *J. Compos. Constr.*, vol. 5, no. 1, pp. 18–25, 2005.

[21] A. F. Ashour and M. N. Habeeb, "Continuous concrete beams reinforced with CFRP bars," *ICE Proc. Struct. Build.*, vol. 161, no. 6, pp. 349–357, 2008.

[22] A. F. Ashour, and M. Family, "Tests of concrete flanged beams reinforced with CFRP bars," *Mag. Concr. Res.*, vol. 58, no. 9, pp. 627–639, 2006.

[23] S. H. Alsayed, Y. A. Al-Salloum, and T. H. Almusallam, "Performance of glass fiber reinforced plastic bars as a reinforcing material for concrete structures," *Compos., Part B Eng.*, vol. 31, pp. 555–567, 2000.

[24] C. Barris, L. Torres, A. Turom, M. Baena, and A. Catalan, "An experimental study of the flexural behavior of GFRP RC beams and comparison with predicted models," *Compos. Struct.*, vol. 91, pp. 286–295, 2009.

[25] M. El-Mogy, A. El-Ragaby, and E. El-Salakawy, "Flexural behavior of continuous FRP-reinforced concrete beams," *J. Compos. Constr.*, vol. 14, no. 6, pp. 669–680, 2010.

[26] G. Thiagarajan, "Experimental and Analytical Behavior of Carbon Fiber-based rods as Flexural Reinforcement," *J. Compos. Constr.*, vol. 7, no. 1, pp. 64–72, 2003.

[27] M. A. Rashid, M. A. Mansur, and P. Paramasivam, "Behavior of aramid fiber-reinforced polymer reinforced high strength concrete beams under bending," *J. Compos. Constr.*, vol. 9, no. 2, pp. 117–127, 2005.

[28] R. K. Kalluri, “Bending behavior of concrete T-beams reinforced with glass-fiber reinforced polymer bars,” Ph.D. dissertation, West Virginia Univ., Morgantown, 1999, 112 p.

[29] H. A. Toutanji and M. Saafi, "Flexural behavior of concrete beams reinforced with glass fiber-reinforced polymer (GFRP) bars," *ACI Struct. J.*, vol. 97, no. 5, pp. 712–719, 2000.

Author contributions: FASB: conceptualization, writing, data curation, formal analysis and methodology; TNB and MMF: conceptualization, funding acquisition, supervision; FRA: conceptualization and methodology; GRB: conceptualization

Editors: Rebecca Gravina, Guilherme Aris Parsekian.